Journal of Materials Chemistry A

PAPER

View Article Online
View Journal | View Issue

Cite this: J. Mater. Chem. A, 2019, 7, 17995

Enabling non-flammable Li-metal batteries *via* electrolyte functionalization and interface engineering†

Jing Yu,‡[a] Yu-Qi Lyu,‡[a] Jiapeng Liu,[a] Mohammed B. Effat,[a] Stephen C. T. Kwok,[ab] Junxiong Wu[a] and Francesco Ciucci *[abc]

Received 10th April 2019
Accepted 9th July 2019

DOI: 10.1039/c9ta03784e

rsc.li/materials-a

Li-metal batteries (LMBs) with composite polymer electrolytes (CPEs) have attracted considerable attention compared with conventional Li-ion batteries. However, the uncontrolled Li deposition and the flammability of CPEs are still pressing issues. In this article, a non-flammable CPE is fabricated. The CPE consists of a poly(vinylidene fluoride) matrix, $Li_{6.4}La_3Zr_{1.4}Ta_{0.6}O_{12}$ fillers, a flame-retardant trimethyl phosphate as the solvent, and a $LiClO_4$ salt. It exhibits unique characteristics, including non-flammability, high ionic conductivity, flexibility, and good thermal stability. A fluoroethylene carbonate (FEC) additive is used on the surface of Li metal to facilitate the formation of a LiF-rich solid electrolyte interphase layer. The FEC-coated Li|CPE|$LiFePO_4$ battery exhibits excellent cycling stability (at room temperature) with a discharge capacity of 152 mA h g^{-1} and nearly 100% coulombic efficiency over 500 cycles at 0.2C. The non-flammable CPE has a high rate capability of 109 mA h g^{-1} at 4C. To improve the energy density of the LMB, the $LiFePO_4$ cathode is replaced with a high-voltage material $LiNi_{1/3}Mn_{1/3}Co_{1/3}O_2$. The obtained Li|CPE|$LiNi_{1/3}Mn_{1/3}Co_{1/3}O_2$ cell exhibits a discharge capacity of 109 mA h g^{-1} after 100 cycles at 0.2C. Consequently, the strategy offers guidelines for the future development of safe batteries with high energy density.

Introduction

Li-ion batteries (LIBs) are predominantly employed in portable electronic devices. However, their current energy density (~300 W h kg^{-1}), is insufficient for the ever-growing demand of electric vehicles, for which an energy density above 500 W h kg^{-1} is needed to ensure long-range mobility with a single charge.[1,2] To increase the energy density of LIBs, one promising approach is to replace the carbon-based anodes (*e.g.*, graphite, 372 mA h g^{-1}) with metallic Li.[3,4] This is because Li has a high theoretical specific capacity (3860 mA h g^{-1}) and a low electrochemical potential (−3.04 V *versus* the standard hydrogen electrode).[5–7] An article of Choi and Aurbach showed that a rechargeable Li-metal battery (LMB) assembled with a metallic Li anode and a high-voltage cathode (*e.g.*, $LiNi_{1/3}Mn_{1/3}Co_{1/3}O_2$) can achieve an energy density of about 500 W h kg^{-1}.[8] However, due to the highly active nature of Li metal, rechargeable LMBs typically cycle poorly and have low coulombic efficiency (CE).[5,9] Furthermore, the uncontrolled deposition of mossy Li increases the risk of various catastrophic processes, such as cracking of the solid electrolyte interphase (SEI), and the continuous decomposition of the electrolytes, thus ultimately leading to battery thermal runaway, fire, and explosion.[10,11] These formidable challenges have stimulated intensive investigations into the utilization of polymer electrolytes, which are more stable with Li metal than liquid electrolytes and can solve the safety issues caused by leakage of the electrolyte.[12,13]

Composite polymer electrolytes (CPEs) possess a relatively high ionic conductivity, good thermal stability and are flexible. Various CPEs, including Al_2O_3-poly(vinylidene fluoride-*co*-hexafluoropropylene) (PVDF-HFP),[14] $Li_{0.33}La_{0.557}TiO_3$-polyacrylonitrile (PAN),[15] $Li_7La_3Zr_2O_{12}$-poly(ethylene oxide) (PEO),[16] $Li_{6.75}La_3Zr_{1.75}Ta_{0.25}O_{12}$-poly(propylene carbonate) (PPC),[17] and $Li_{6.75}La_3Zr_{1.75}Ta_{0.25}O_{12}$-PVDF,[18] have been widely exploited. For example, Shen *et al.* reported that N atoms of the *N*,*N*-dimethylformamide (DMF) solvent complexes with La atoms in LLZTO.[18] This process activates the interaction between PVDF and LLZTO, leading to the partial dehydrofluorination of PVDF and boosting the ionic conductivity. CPEs have also shown to be capable of suppressing or delaying the growth of Li dendrites.[19,20] However, previously reported CPEs usually incorporate highly flammable organic solvents (*e.g.*, ether-based

[a]Department of Mechanical and Aerospace Engineering, The Hong Kong University of Science and Technology, Hong Kong, China SAR. E-mail: francesco.ciucci@ust.hk

[b]Guangzhou HKUST Fok Ying Tung Research Institute, China

[c]Department of Chemical and Biological Engineering, The Hong Kong University of Science and Technology, Hong Kong, China SAR

† Electronic supplementary information (ESI) available. See DOI: 10.1039/c9ta03784e

‡ These authors contributed equally to this work.

solvents), which might be easily ignited.[18,21] Meanwhile, various groups have developed non-flammable liquid electrolytes, including ionic liquids,[22] fluoroethers,[23] and organosilicon compounds,[24] or used flame-retardant additives, including compounds containing phosphorus or fluorine, such as trimethyl phosphate (TMP), triethyl phosphate (TEP), diethyl ethylphosphonate (DEEP), and dimethyl methyl phosphonate (DMMP).[25,26] These studies on liquid electrolytes certainly represent a database for the choice of an appropriate non-flammable solvent for CPEs. It is important to note that, to date, there are no studies introducing non-flammable solvents into CPEs to overcome the aforementioned drawbacks.

Recently, Yamada *et al.* developed safe and long-lasting liquid-based LIBs, using the flame-retardant TMP, as the sole solvent.[25] These authors obtained excellent cycling stability, which was attributed to the formation of an inorganic SEI enabled by the high salt concentration in the TMP (5.3 M $LiN(SO_2F)_2$/TMP). However, while the extremely high salt concentration is beneficial to the stability, it is costly and it significantly increases the electrolyte viscosity, leading to an under-utilization of active materials.[26,27] The previous study by Yamada and co-workers supports the viability of using non-flammable TMP as solvent for the LIBs and highlights the need of optimizing the salt concentration. Generally, the introduction of flame retarding solvents into liquid-based electrolytes results in a compromised cell performance since those solvents do not suitably passivate commonly used anodes. For example, we note that TMP is not electrochemically stable with Li metal.[26,28] This requires engineering the interface between the CPE and Li metal. Rationally developing a safe CPE that is also compatible with Li metal is the objective of this study.

Herein, we have prepared a novel CPE membrane (Fig. 1) based on the PVDF polymer matrix, using TMP as the solvent, $Li_{6.4}La_3Zr_{1.4}Ta_{0.6}O_{12}$ (LLZTO) as the ceramic filler, and $LiClO_4$ as the lithium salt. Our CPE is free-standing and exhibits unique characteristics, including non-flammability, high flexibility, and good thermal stability. We also engineered the Li–CPE interface by adding fluoroethylene carbonate (FEC), which effectively enhances the uniform Li deposition on the electrode surface and improves the stability of the overall battery, thanks to the formation of a LiF-rich SEI layer. The assembled symmetric Li|CPE|Li cells with the FEC-protected Li-metal anode have a long cycle life, exhibiting a stable voltage response at 0.2 mA cm^{-2} for over 500 h. Moreover, a Li|CPE|$LiFePO_4$ (LFP) cell with the FEC-protected Li anode has excellent cycling stability with a CE of 99.8% over 500 cycles. Noticeably, long-term cycling at 1C of a battery can still deliver a discharge capacity of 144 mA h g^{-1} with a capacity retention of 99.3% after 300 cycles at room temperature (RT).

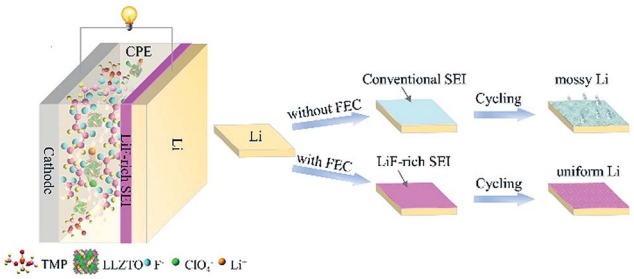

Fig. 1 Schematic showing a CPE membrane composed of PVDF, LLZTO, TMP, and $LiClO_4$. A LiF-rich SEI layer, which forms between the Li-metal anode and the CPE membrane, enhances the uniform deposition of Li and impedes the decomposition of the electrolyte.

Experimental section

Materials synthesis

The LLZTO powder was prepared by a solid–state reaction, as described elsewhere.[29] Stoichiometric amounts of $LiOH\cdot H_2O$ (≥99.0%, Sigma-Aldrich), La_2O_3 (99%, <100 nm, Sigma-Aldrich), ZrO_2 (<100 nm, Sigma-Aldrich), and Ta_2O_5 (≥99.99%, Ourchem) were mixed and ball milled in isopropanol for 90 min at 500 rpm. Then, the mixture was heated inside a MgO crucible in air at 900 °C for 12 h. We added to the mix an extra 10 wt% of $LiOH\cdot H_2O$ to compensate for the loss of Li and 0.3 wt% of Al_2O_3 as a sintering aid.[30] The powder was then ground and pressed into pellets. After that, the pellets were covered with the mother powder and annealed at 1140 °C for 16 h. Finally, the LLZTO pellets were reground into powder and added to CPE.

Free-standing CPEs were prepared by mixing 0.15 g of dried $LiClO_4$ (99.99%, Sigma-Aldrich), 0.05 g of the LLZTO powder, and 0.45 g of PVDF (Kynar HSV900, Arkema) into the 6.0 mL of TMP solution (Shanghai Zhanyun Chemical Co. Ltd., 98%). This recipe was proposed following our previous work.[31] The mixture was then stirred at 60 °C for 10 h on a hot plate to form a viscous

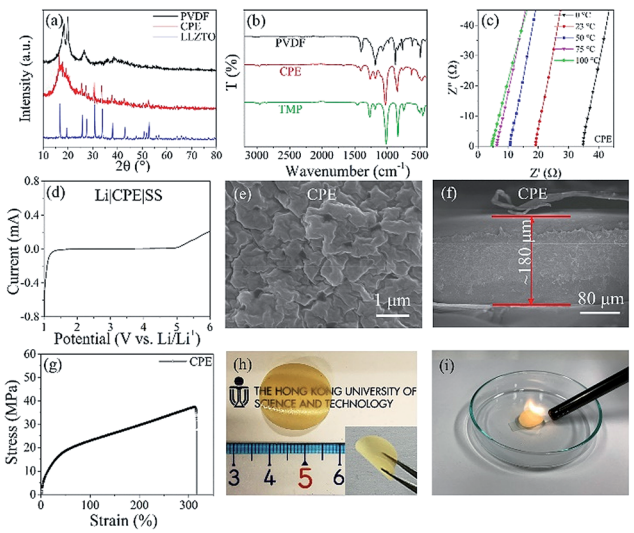

Fig. 2 (a) XRD patterns of PVDF, CPE, and the LLZTO powder. (b) FTIR spectra of PVDF, CPE, and TMP. (c) EIS of the symmetric SS|CPE|SS cell at different temperatures. (d) LSV of the Li|CPE|SS cell. (e) Top and (f) cross-sectional SEM images of the CPE membrane. (g) A stress–strain curve of the CPE membrane. (h) Digital photographs of the flexible and translucent CPE membrane. (i) Evaluation of the flammability of the CPE membrane.

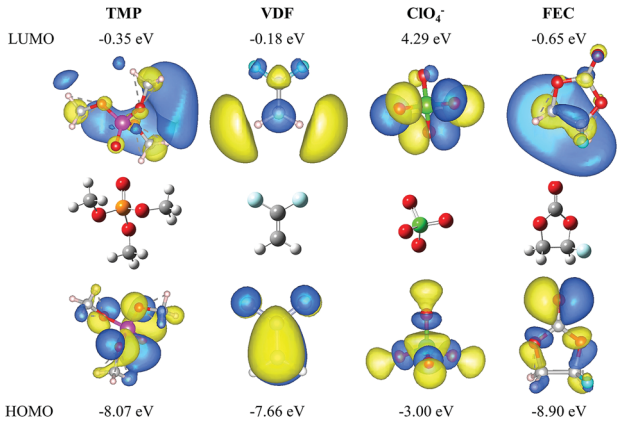

Fig. 3 The LUMO and HOMO energy values of TMP, VDF, ClO_4^- and FEC obtained by DFT.

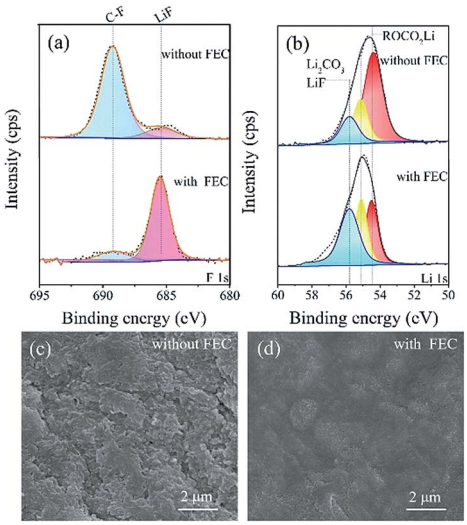

Fig. 5 XPS spectra and SEM images of the SEI layer. (a) F 1s and (b) Li 1s XPS spectra of the surface of the Li anode without FEC coating after 28 cycles (the failure of the symmetric cell), and with FEC coating after 100 cycles. SEM images of the surface of the Li anode (c) without FEC coating after 28 cycles and (d) with the FEC coating after 100 cycles.

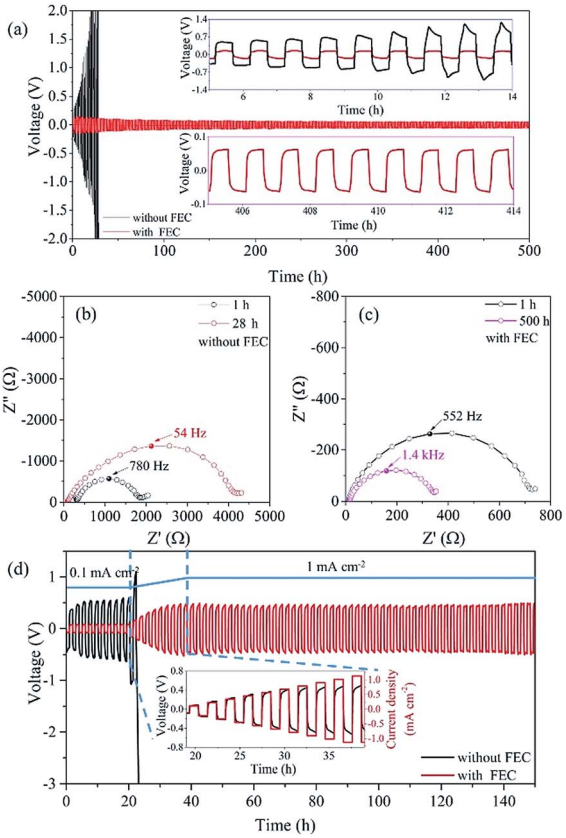

Fig. 4 (a) Cycling stability of the Li|CPE|Li symmetric cells with and without FEC coating at a current density of ±0.2 mA cm^{-2}. EIS of Li|CPE|Li cells (b) without and (c) with the FEC coating before and after cycling. (d) Cycling stability of the symmetric cells without and with the FEC coating at current densities from 0.1 to 1 mA cm^{-2}.

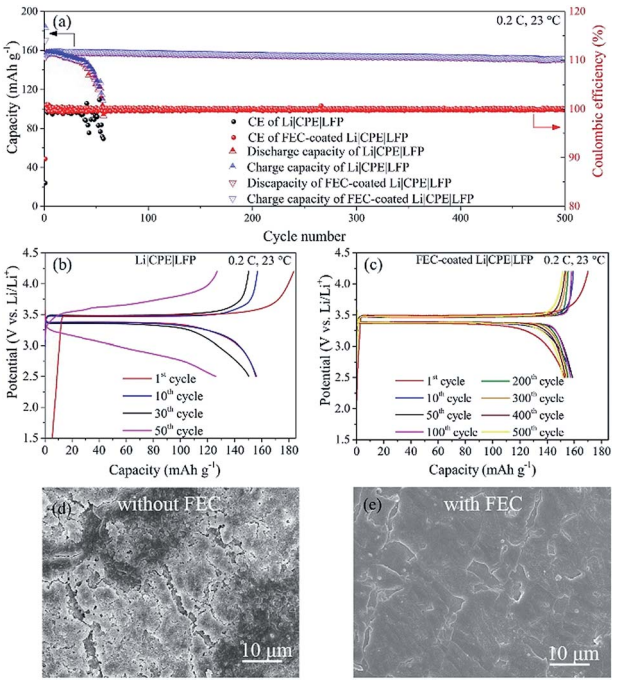

Fig. 6 (a) Cycling performance of Li|CPE|LFP cells without and with FEC coating at 0.2C. The charge/discharge curves of Li|CPE|LFP cells (b) without and (c) with FEC coating. SEM images of the surface of the Li-metal anode (d) without and (e) with FEC.

solution. Finally, the obtained mixture was poured onto a glass dish and immediately placed in a vacuum oven for 10 h at 60 °C. The electrolyte membrane thickness was measured to be 150–200 μm.

The cathode was fabricated by mixing the active material, Super-P carbon black (MTI, TIMICAL SUPER C65) and PVDF in *N*-methyl-2-pyrrolidone (NMP, MTI, 99.9%). For the preparation of LFP and $LiNi_{1/3}Mn_{1/3}Co_{1/3}O_2$ (NMC111) electrodes, the weight ratio of LFP (Aleees, Taiwan) or NMC111 (Bamo-tech, Tianjin)/Super-P carbon black/PVDF was at 8 : 1 : 1. Then, the obtained slurries were cast on an Al foil and dried at 110 °C in

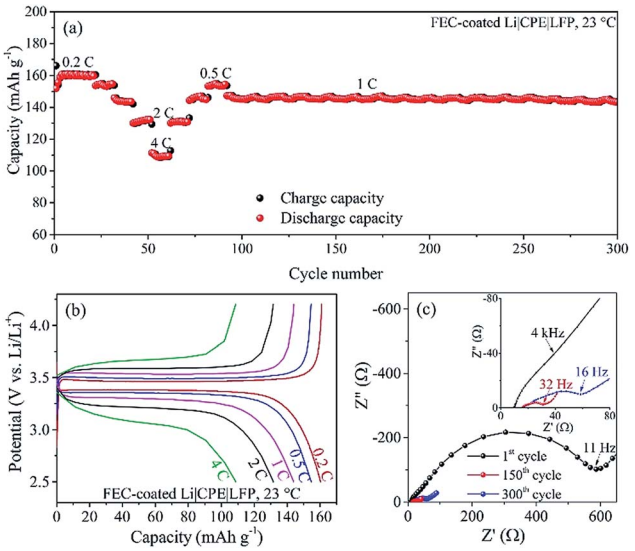

Fig. 7 (a) Rate performance of a Li|CPE|LFP cell with FEC at 0.2C, 0.5C, 1C, 2C, and 4C. (b) Typical charge–discharge curves of a Li|CPE|LFP cell with FEC at different C-rates (the typical curves at 0.2C, 0.5C, 1C, 2C and 4C are the 10th, 30th, 40th, 50th, and 60th cycles, respectively). (c) EIS of a Li|CPE|LFP cell with FEC at the 1st, 150th, and 300th cycle.

an oven for 12 h. Finally, the Al foil with the cathode layer (active material mass loading of 2–3 mg cm^{-2}) was cut into 12.0 mm diameter disks. Regarding the FEC coating, the surface of the Li-metal was first wetted with 2.0 μL of FEC and then dried at RT for half an hour in the glovebox.

Material characterizations

The phase structure of the LLZTO powder and the CPE membrane was determined by X-ray diffraction (XRD, PANalytical Empyrean) with Cu Kα ($\lambda = 1.5406$ Å) radiation in the 2θ range from 10 to 90°. Fourier transform infrared (FTIR, VERTEX 70) spectra were recorded to confirm the presence of TMP in PVDF. The surface composition of the Li-metal anode before and after cycling was measured by X-ray photoelectron spectroscopy (XPS, PHI 5600). The morphology of the Li-metal anode and the CPE membrane was recorded using scanning electron microscopy (SEM, JEM 6700F). The Li-metal anodes obtained from the disassembled cell were first cleaned by diethyl carbonate (DEC) solvent for three times and dried overnight in the glovebox. Thermo-gravimetric analysis (TGA, Q5000-TA) was carried out from RT to 550 °C at a heating rate of 10 °C min^{-1} in N_2 (99.996%, Air Products). To avoid side reactions with air, all samples were kept in Ar before characterization.

Electrochemical characterizations

The impedance of the CPE membrane between the stainless steel (SS) disks (SS|CPE|SS) was measured in a CR2032 coin cell using the electrochemical impedance spectroscopy (EIS) with an electrochemical workstation (VSP-300, Bio-Logic). The ionic conductivity (σ) was calculated based on the relation $\sigma = l/RA$, where l is the thickness of the electrolyte membrane, R is the measured resistance, and A is the surface area of the electrolyte. The activation energy (E_a) was calculated according to the Arrhenius equation $\sigma(T) = A\exp(-E_a/RT)$, where A is a pre-exponential factor and T is the absolute temperature. The charge–discharge curves and cycling stability of Li/LFP and Li/NMC111 cells were measured in the range from 2.5 to 4.2 V and 2.8 to 4.5 V respectively, using a battery testing system (CT2001A, LANHE, China). All preparation procedures were conducted inside a glovebox (Mikrouna, $[O_2] < 0.1$ ppm, $[H_2O] < 0.1$ ppm) filled with ultrapure Ar (≥99.999%, Air products).

Density functional theory calculations

All the density functional theory (DFT) calculations were carried out with a hybrid B3LYP functional[32] as implemented in Gaussian 09.[33] The 6-31++G (d,p) basic set was used in all computations. First, structures of all molecules were optimized, and the vibrational frequencies were calculated. The energy of molecular orbitals was carried out based on the optimized structure, and the highest occupied molecular orbital (HOMO) and lowest unoccupied molecular orbital (LUMO) are visualized using the GaussView software.[34]

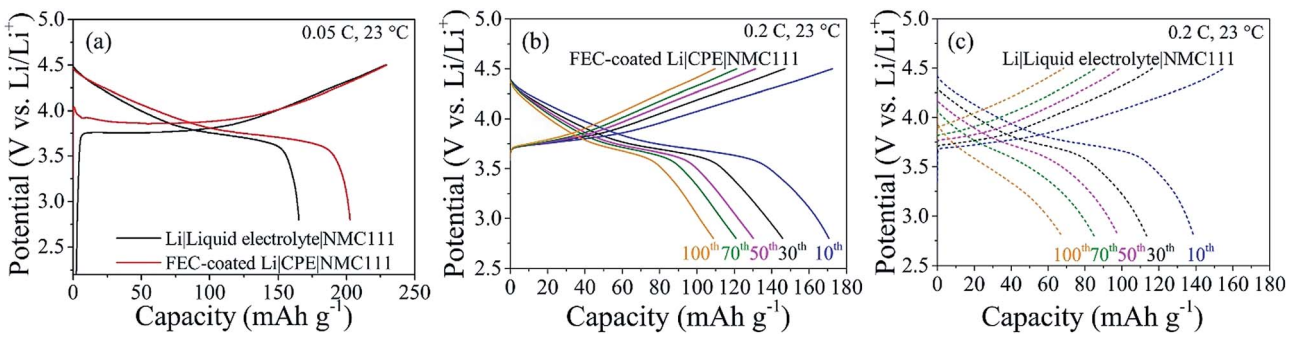

Fig. 8 (a) First charge–discharge profiles of the FEC-coated Li|CPE|NMC111 cell and Li|liquid electrolyte|NMC111 cell. Typical charge–discharge profiles of the (b) FEC-coated Li|CPE|NMC111 and (c) Li|liquid electrolyte|NMC111 batteries. Both cells were first charged and discharged at 0.05C for 8 cycles and then cycled 100 times at 0.2C.

Results and discussion

Non-flammable composite polymer electrolyte

The CPE membrane was fabricated by solution casting thoroughly mixed components, *i.e.*, PVDF, LLZTO, TMP, and $LiClO_4$ (Fig. 1). The phase structures of PVDF, LLZTO, and CPE were determined by XRD. As shown in Fig. 2a, the LLZTO powder employed in the CPE membrane has a cubic phase without detectable impurities (Fig. 2a & S1a†). Such a cubic phase is preferred due to its intrinsically higher ionic conductivity compared with that of the tetragonal phase of LLZTO.[35] Also, the XRD pattern suggests that the cubic LLZTO is well preserved in the CPE membrane. In contrast, the PDVF's phase appears to change from the nonpolar α phase to a combination of the polar β and γ phases. This is evidenced by the CPE's XRD pattern where the PVDF's peaks at ~18.4°, ~20.1°, and ~26.7° are replaced by a new broad peak with a clear shoulder peak at ~20.2°.[36,37] We should note that the higher polarity has been shown to benefit for the salt dissociation and the Li-ion migration within CPE.[38,39] Fig. 2b shows the FTIR spectra of PVDF, TMP, and CPE. The characteristic peaks of PVDF (510 cm^{-1} and 840 cm^{-1})[40] and TMP (1016 cm^{-1} and 1463 cm^{-1})[41] are preserved in the FTIR spectrum of the CPE membrane, confirming the presence of PVDF and TMP.

The ionic conductivity of the ceramic LLZTO pellet and CPE membrane was estimated by EIS. As shown in Fig. S1b,† an LLZTO pellet with a thickness of 0.94 mm and a diameter of 12.45 mm has a resistance of ~380 Ω. The corresponding RT ionic conductivity is calculated to be $\sim 2 \times 10^{-4}$ S cm^{-1}, a value comparable to those reported for LLZTO in the literature.[30,35] The EIS spectra of the CPE membrane were measured at various temperatures, see Fig. 2c. Consequently, the ionic conductivity could be calculated. For instance, the ionic conductivity of CPE at RT is estimated to be 4.7×10^{-4} S cm^{-1}, given the bulk resistance of 19 Ω, a thickness of 180 μm, and a diameter of 16 mm. According to the Arrhenius plot of CPE (Fig. S2a†), the activation energy of CPE is as low as 0.208 eV, suggesting the fast Li^+ migration.[18] The electrochemical stability against the reduction and oxidation is also critical for polymer electrolytes. The electrochemical window of CPE was studied by linear sweep voltammetry (LSV) in the range of 1.0–6.0 V using Li metal and SS electrodes (Fig. 2d). No oxidation peaks of the SS|CPE|Li cell can be observed at the potential as high as 4.5 V (*vs.* Li/Li^+). Moreover, a negligible current (<3 μA) was observed at 4.5 V and 4.8 V (*versus* Li/Li^+) in chronoamperometry measurements (Fig. S2b†). These results indicate that the obtained CPE is redox inactive and the corresponding SS|CPE|Li cell has a wide working potential window.

The top and cross-sectional views of the CPE membrane taken by SEM are presented in Fig. 2e and f. The CPE membrane shows a well-connected and relatively dense microstructure with a thickness of ~180 μm. SEM and the corresponding energy-dispersive X-ray spectroscopy (EDS) mapping images are shown in Fig. S3,† indicating a seemingly uniform distribution of PVDF (F), LLZTO (Ta), TMP (P), and $LiClO_4$ (Cl).

A typical stress–strain curve for the CPE membrane is presented in Fig. 2g. The CPE membrane shows a tensile strength of 37.3 MPa, comparable to that of PVDF-based membranes,[31] and much higher than those recorded for PEO-based electrolytes, such as PEO–$LiClO_4$ (0.35 MPa)[42] and $(PEO)_8$LiTFSI (10 MPa).[43] Fig. 2h shows digital photographs of the free-standing CPE, which appears to be translucent and flexible. The flammability of the electrolyte is another essential characteristic that directly affects battery safety. As shown in Fig. 2i, the obtained CPE membrane with the addition of TMP is non-flammable. In contrast, a CPE membrane prepared with *N*,*N*-dimethylformamide (DMF) easily catches fire (Fig. S4†). This behavior confirms that the obtained CPE membrane composed of TMP as the solvent has a far stronger fire-resistance than an analogous CPE membrane with a flammable organic liquid as the solvent.

The thermal stability of the PVDF powder and the CPE membrane was further assessed by TGA. As shown in Fig. S5,† the decomposition of PVDF occurs at ~460 °C, in agreement with the literature,[18] while the weight loss of the CPE membrane starts at ~100 °C. The reduced decomposition temperature is attributed to the low-boiling point of TMP (197 °C) in the CPE membrane.[44] In addition, the prolonged weight loss between 100 to 269 °C is plausibly due to the TMP solvent enclosed in the PVDF matrix.[45] In addition, the CPE membrane experiences sharp weight losses at ~269, ~340, and ~446 °C. The weight loss starting at 446 °C is attributable to the decomposition of the PVDF matrix. Although the thermal decomposition of the CPE membrane starts around 100 °C, this value is still higher than that of conventional liquid organic electrolytes. For example, the thermal decomposition of LiTFSI in ethylene carbonate (EC) and dimethyl carbonate (DMC) begins at 80 °C.[46]

FEC-induced SEI layer

Although the TMP solvent makes the CPE membrane non-flammable, TMP itself is reported to be unstable against Li metal.[26,28] As a result, the discharge capacity might be drastically reduced during cycling.[27] FEC has been reported as an additive capable of promoting the formation of effective SEI layers on Li metal,[47] graphite,[48] and silicon.[49] Therefore, we coated the Li anode with FEC, to promote the formation of a stable passivation layer that overcomes the challenge of TMP contacting directly with the Li metal. To demonstrate the creation of an SEI layer, the chemical composition of the Li surface with and without the FEC coating was investigated by XPS. As shown in Fig. S6,† a characteristic peak of LiF (55.7 eV) can be observed in the FEC-coated Li-metal anode.

To further understand the formation of the FEC-induced LiF-rich SEI layer, we carried out *ab initio* calculations. We calculated the energy of HOMO and LUMO of TMP, vinylidene difluoride (VDF), ClO_4^- and FEC by DFT. As shown in Fig. 3, FEC (−0.65 eV) has a lower LUMO energy, suggesting a greater tendency for FEC to be reduced on the surface of Li metal. In addition, FEC (−8.90 eV) has the lowest HOMO energy, indicating a lower reactivity at positive potentials.[50] These results suggest that, among all CPE components, FEC will tend to be preferentially decomposed.

Electrochemical performance

To assess the compatibility between Li and CPE with and without FEC, we carried out Li plating and stripping experiments for 1 h in one cycle using Li symmetrical cells which were subjected to a current density of ± 0.2 mA cm^{-2} (Fig. 4a). Without the FEC coating, the overpotential of Li plating and stripping increases dramatically and exceeds ± 2 V after 28 h. In contrast, the FEC-coated Li/Li cell shows a gradual decrease of the potential in the early cycles with the voltage stabilizing at $\sim$70 mV after 500 h.

The EIS of the symmetric cells before and after cycling are shown in Fig. 4b and c. It is worth noting that the introduction of FEC reduces the total resistance of the cells. As shown in Fig. 4b, after 28 cycles, the total resistance of the Li/Li cell without the FEC coating is much higher than that measured in the first cycle, increasing from $\sim$1870 to $\sim$4250 Ω. However, as shown in Fig. 4c, the total resistance of the FEC-coated symmetric cell is $\sim$730 Ω in the first cycle, decreasing to $\sim$345 Ω after 500 cycles. Such a reduction is mainly ascribed to the formation of the LiF-containing SEI layer.

Moreover, we found that the cell without FEC displayed a substantial increase in overpotential at higher current densities. For example, the overpotential exceeds 3 V when the current density is 0.3 mA cm^{-2} (Fig. 4d). In contrast, the Li/Li cell with the FEC coating could still run stably for over 150 h at a current density as high as 1 mA cm^{-2} (Fig. 4d). The excellent cyclability of the cell with FEC is likely related to the formation of a uniform LiF-rich SEI layer at the electrode/electrolyte interface.[51,52]

XPS analysis was conducted to assess the chemical species of the surface of the Li-metal anode in Li/Li cells with and without the FEC coating after experiencing certain cycles. As shown in Fig. 5a, the F 1s spectra have two characteristic peaks, which can be assigned to LiF (685.5 eV) and C–F (689.2 eV), respectively.[53] According to the peak area, the proportion of LiF (76.7%) on the surface of the Li anode after coating with FEC is significantly higher than that (12.8%) measured for the Li anode without FEC. According to the Li 1s spectra (Fig. 5b), the content of LiF (55.7 eV)[47] also increases with the addition of FEC, suggesting the formation of LiF after introducing FEC. We should note that LiF is an electrical insulator with low electrical conductivity in the order of $\sim 10^{-31}$ S cm^{-1}.[54] Therefore, the formed LiF-rich SEI interface can effectively block the transfer of electrons and thus prevent the electrochemical decomposition of the electrolyte.[47]

The morphology of the Li-metal anode in the symmetric cell after plating and stripping was imaged by SEM (Fig. 5c and d). As shown in Fig. 5c, the surface of the Li foil appears rough if FEC is absent, indicating the uneven deposition of Li during the plating and stripping process. In contrast, the FEC-induced SEI significantly reduces the accumulation of the dead Li, leading to a seemingly uniform and smooth surface without any mossy Li deposited on its surface (Fig. 5d).

We also investigated the charge–discharge and cycling performance of Li/LFP cells (Fig. 6). The Li/LFP cell with FEC coating has significantly improved cycling stability compared to the FEC-free cell. In the initial 20 cycles, both batteries deliver a similar reversible capacity at 0.2C, but the reversible capacity of the FEC-free cell declines sharply after 40 cycles, and the discharge capacity drops below 100 mA h g^{-1} after only 55 cycles (Fig. 6a). Such a capacity loss is likely due to the instability of TMP with the Li-metal anode as reported previously by the Wang and Xu groups,[28,55] and a large polarization during discharge prevents the battery from achieving a reasonable capacity (Fig. 6b). In contrast, the FEC-coated Li/LFP cell exhibits a flat charge/discharge voltage plateau with a potential gap of 0.1244 V at 0.2C (Fig. 6c). The cell also displays an initial CE of 89.8% and excellent cycling stability. Even after 500 cycles at 0.2C, a discharge capacity of 152 mA h g^{-1} and a high CE of $\sim$99.8% could still be maintained. Interestingly, the discharge capacity of this battery increases from 153 mA h g^{-1} to 157 mA h g^{-1} during the initial 10 cycles (Fig. 6c). This phenomenon is explained by the optimization of the electrolyte/electrode interfaces as shown in other literature reports.[56,57] The SEM images (Fig. 6d and e) of the Li-metal surface of the Li/LFP batteries without and with FEC also support the FEC hypothesis mentioned above. As shown in Fig. 6d, the surface of the Li-metal anode without FEC is relatively porous after experiencing 50 cycles at 0.2C. In contrast, the Li anode with FEC appears denser and smoother under similar testing conditions (Fig. 6e), indicating a uniform Li deposition.

The FEC-coated battery also has excellent rate performance (Fig. 7a). As shown in Fig. 7b, the battery with FEC achieves discharge capacities of 160 mA h g^{-1} at 0.2C, 154 mA h g^{-1} at 0.5C, 144 mA h g^{-1} at 1C, 131 mA h g^{-1} at 2C, and 109 mA h g^{-1} at 4C at RT, and the anomalous black points in the charge capacity are likely due to C-rate switch. When the current density goes back to 1C, the capacity remains at 143 mA h g^{-1} with a capacity retention of 99.3% after 300 cycles (Fig. 7a), exhibiting excellent operational stability. The corresponding resistances are shown in Fig. 7c. The resistance decreases drastically after 150 cycles and increases slightly from the 150^{th} cycle to the 300^{th} cycle (Fig. 7c). The Li/LFP cell assembled with our CPE and an FEC-protected Li anode exhibits a superior discharge capacity and outstanding capacity retention in comparison with recent works, as summarized in Table S1.†

Furthermore, the wide electrochemical stability window of the prepared CPE membrane (Fig. 2d & S2b†) has prompted us to explore high-voltage cathode materials such as $LiNi_{1-x}M_xO_2$ (M = transition metal), and $LiCoPO_4$.[58–60] To further support the claim that the CPE membrane is stable at high voltages, we made a CPE with NMC111 as the cathode and FEC-coated Li-metal as the anode. We evaluated this battery between 2.8 and 4.5 V. For comparison, a traditional Li|NMC111 cell with liquid electrolyte (1.0 M $LiPF_6$ with 1.0% vinylene carbonate in EC : DMC : ethylmethyl carbonate (EMC) = 1 : 1 : 1, v/v) was also prepared and tested. Even though both cells had a similar first cycle charge capacity, the Li|CPE|NMC111 cell with FEC exhibited a much higher initial discharge capacity (203 mA h g^{-1} with a CE of 88.4% at 0.05C) compared to the Li|liquid electrolyte|NMC111 cell (165 mA h g^{-1} with a CE of 72.3%) as shown in Fig. 8a. Fig. 8b and c further show the charge–discharge profiles of different cycles at 0.2C. Compared with the Li|liquid electrolyte|NMC111, the FEC-coated

Li|CPE|NMC111 cell has a lower voltage polarization and a smaller capacity decay, suggesting a significant improvement. The battery with the prepared CPE can maintain its discharge capacity at 109 mA h g^{-1} after 100 cycles, a value much higher than that of the battery with the liquid electrolyte (67 mA h g^{-1}).

Conclusions

In this study, we have successfully developed a free-standing, flexible, and non-flammable Li-ion conductive CPE. We also modified the surface of the Li metal with a coating of FEC and demonstrated, by physical characterizations and DFT simulations, that a LiF-rich SEI layer forms to protect the Li metal anode. A Li|CPE|LFP battery with FEC coating exhibits good cycling stability and excellent rate capability, as demonstrated by a discharge capacity of 152 mA h g^{-1} with CE of 99.8% over 500 cycles at 0.2C at RT, as well as the discharge capacities of 144 mA h g^{-1} at 1C, 131 mA h g^{-1} at 2C, and 109 mA h g^{-1} at 4C. Furthermore, we investigated the compatibility of the prepared CPE with an NMC111 high voltage cathode. We obtained a stable CE of ~98.9% and a discharge capacity of 109 mA h g^{-1} after 100 cycles. Our findings provide an effective strategy to resolve the safety and stability issues of LMBs.

Conflicts of interest

There are no conflicts to declare.

Acknowledgements

The authors gratefully acknowledge the Research Grants Council of Hong Kong for support through the projects (16207615, 16227016, and 16204517). The authors also acknowledge the support from the Guangzhou Science and Technology Program (No. 201807010074), and Hong Kong Innovation and Technology Fund (No. ITS/292/18FP).

Notes and references

1 X. Fan, L. Chen, X. Ji, T. Deng, S. Hou, J. Chen, J. Zheng, F. Wang, J. Jiang, K. Xu and C. Wang, *Chem*, 2018, **4**, 174–185.
2 S. Chen, K. Wen, J. Fan, Y. Bando and D. Golberg, *J. Mater. Chem. A*, 2018, **6**, 11631–11663.
3 Y. Sun, N. Liu and Y. Cui, *Nat. Energy*, 2016, **1**, 16071.
4 Z. Lu, J. Yu, J. Wu, M. B. Effat, S. C. T. Kwok, Y. Lyu, M. M. F. Yuen and F. Ciucci, *Energy Storage Materials*, 2019, **18**, 311–319.
5 D. Lin, Y. Liu and Y. Cui, *Nat. Nanotechnol.*, 2017, **12**, 194–206.
6 X.-B. Cheng, R. Zhang, C.-Z. Zhao, F. Wei, J.-G. Zhang and Q. Zhang, *Adv. Sci.*, 2016, **3**, 1500213.
7 Y. Liu, Q. Liu, L. Xin, Y. Liu, F. Yang, E. A. Stach and J. Xie, *Nat. Energy*, 2017, **2**, 17083.
8 J. W. Choi and D. Aurbach, *Nat. Rev. Mater.*, 2016, **1**, 16013.
9 W. Xu, J. Wang, F. Ding, X. Chen, E. Nasybulin, Y. Zhang and J.-G. Zhang, *Energy Environ. Sci.*, 2014, **7**, 513–537.
10 H. Duan, Y.-X. Yin, Y. Shi, P.-F. Wang, X.-D. Zhang, C.-P. Yang, J.-L. Shi, R. Wen, Y.-G. Guo and L.-J. Wan, *J. Am. Chem. Soc.*, 2018, **140**, 82–85.
11 H. Wu, D. Zhuo, D. Kong and Y. Cui, *Nat. Commun.*, 2014, **5**, 5193.
12 L. Yue, J. Ma, J. Zhang, J. Zhao, S. Dong, Z. Liu, G. Cui and L. Chen, *Energy Storage Materials*, 2016, **5**, 139–164.
13 E. Quartarone and P. Mustarelli, *Chem. Soc. Rev.*, 2011, **40**, 2525–2540.
14 Z. Tu, Y. Kambe, Y. Lu and L. A. Archer, *Adv. Energy Mater.*, 2014, **4**, 1300654.
15 W. Liu, N. Liu, J. Sun, P.-C. Hsu, Y. Li, H.-W. Lee and Y. Cui, *Nano Lett.*, 2015, **15**, 2740–2745.
16 J. Zhang, N. Zhao, M. Zhang, Y. Li, P. K. Chu, X. Guo, Z. Di, X. Wang and H. Li, *Nano Energy*, 2016, **28**, 447–454.
17 J. Zhang, X. Zang, H. Wen, T. Dong, J. Chai, Y. Li, B. Chen, J. Zhao, S. Dong, J. Ma, L. Yue, Z. Liu, X. Guo, G. Cui and L. Chen, *J. Mater. Chem. A*, 2017, **5**, 4940–4948.
18 X. Zhang, T. Liu, S. F. Zhang, X. Huang, B. Q. Xu, Y. H. Lin, B. Xu, L. L. Li, C. W. Nan and Y. Shen, *J. Am. Chem. Soc.*, 2017, **139**, 13779–13785.
19 R. Khurana, J. L. Schaefer, L. A. Archer and G. W. Coates, *J. Am. Chem. Soc.*, 2014, **136**, 7395–7402.
20 W. Zhou, S. Wang, Y. Li, S. Xin, A. Manthiram and J. B. Goodenough, *J. Am. Chem. Soc.*, 2016, **138**, 9385–9388.
21 W. Zhang, J. Nie, F. Li, Z. L. Wang and C. Sun, *Nano Energy*, 2018, **45**, 413–419.
22 G. Kim, S. Jeong, M. Joost, E. Rocca, M. Winter, S. Passerini and A. Balducci, *J. Power Sources*, 2011, **196**, 2187–2194.
23 S. Fang, G. Wang, L. Qu, D. Luo, L. Yang and S.-i. Hirano, *J. Mater. Chem. A*, 2015, **3**, 21159–21166.
24 T. Yong, J. Wang, Y. Mai, X. Zhao, H. Luo and L. Zhang, *J. Power Sources*, 2014, **254**, 29–32.
25 J. Wang, Y. Yamada, K. Sodeyama, E. Watanabe, K. Takada, Y. Tateyama and A. Yamada, *Nat. Energy*, 2018, **3**, 22–29.
26 Z. Zeng, V. Murugesan, K. S. Han, X. Jiang, Y. Cao, L. Xiao, X. Ai, H. Yang, J.-G. Zhang and M. L. Sushko, *Nat. Energy*, 2018, **3**, 674–681.
27 K. Matsumoto, K. Nakahara, K. Inoue, S. Iwasa, K. Nakano, S. Kaneko, H. Ishikawa, K. Utsugi and R. Yuge, *J. Electrochem. Soc.*, 2014, **161**, A831–A834.
28 X. Wang, E. Yasukawa and S. Kasuya, *J. Electrochem. Soc.*, 2001, **148**, A1058–A1065.
29 M. Saccoccio, J. Yu, Z. Lu, S. C. Kwok, J. Wang, K. K. Yeung, M. M. Yuen and F. Ciucci, *J. Power Sources*, 2017, **365**, 43–52.
30 Y. Wang, P. Yan, J. Xiao, X. Lu, J.-G. Zhang and V. L. Sprenkle, *Solid State Ionics*, 2016, **294**, 108–115.
31 J. Yu, S. C. T. Kwok, Z. Lu, M. B. Effat, Y.-Q. Lyu, M. M. F. Yuen and F. Ciucci, *ChemElectroChem*, 2018, **5**, 2873–2881.
32 A. D. Becke, *J. Chem. Phys.*, 1993, **98**, 5648–5652.
33 M. Frisch, G. Trucks, H. B. Schlegel, G. E. Scuseria, M. A. Robb, J. R. Cheeseman, G. Scalmani, V. Barone, B. Mennucci and G. Petersson, *Gaussian 09, Revision A.02*, Gaussian Inc., Wallingford, CT, 2009, p. 200.
34 R. Dennington, T. Keith and J. Millam, *GaussView, Version 6*, Semichem Inc., Shawnee Mission, KS, 2009.

35 R. Murugan, V. Thangadurai and W. Weppner, *Angew. Chem., Int. Ed.*, 2007, **46**, 7778–7781.
36 S. K. Karan, R. Bera, S. Paria, A. K. Das, S. Maiti, A. Maitra and B. B. Khatua, *Adv. Energy Mater.*, 2016, **6**, 1601016.
37 S. Jana, S. Garain, S. Sen and D. Mandal, *Phys. Chem. Chem. Phys.*, 2015, **17**, 17429–17436.
38 F. Wang, L. Li, X. Yang, J. You, Y. Xu, H. Wang, Y. Ma and G. Gao, *Sustainable Energy Fuels*, 2018, **2**, 492–498.
39 M. Kundu, C. M. Costa, J. Dias, A. Maceiras, J. L. Vilas and S. Lanceros-Méndez, *J. Phys. Chem. C*, 2017, **121**, 26216–26225.
40 P. Martins, A. Lopes and S. Lanceros-Mendez, *Prog. Polym. Sci.*, 2014, **39**, 683–706.
41 K. Solangi, A. Amiri, M. Luhur, S. A. A. Ghavimi, S. Kazi, A. Badarudin and M. N. M. Zubir, *RSC Adv.*, 2016, **6**, 4552–4563.
42 L. Fan, C.-W. Nan and M. Li, *Chem. Phys. Lett.*, 2003, **369**, 698–702.
43 A. Arya and A. Sharma, *J. Phys. D: Appl. Phys.*, 2017, **50**, 443002.
44 H. Liu, P. Dai, J. Zhang, C. Zhang, N. Bao, C. Cheng and L. Ren, *Chem. Eng. J.*, 2013, **228**, 425–434.
45 M. M. Nasef and H. Saidi, *Mater. Chem. Phys.*, 2006, **99**, 361–369.
46 H. W. Kim, P. Manikandan, Y. J. Lim, J. H. Kim, S.-C. Nam and Y. Kim, *J. Mater. Chem. A*, 2016, **4**, 17025–17032.
47 X. Q. Zhang, X. B. Cheng, X. Chen, C. Yan and Q. Zhang, *Adv. Funct. Mater.*, 2017, **27**, 1605989.
48 D. Y. Wang, N. Sinha, J. Burns, C. Aiken, R. Petibon and J. Dahn, *J. Electrochem. Soc.*, 2014, **161**, A467–A472.
49 C. Xu, F. Lindgren, B. Philippe, M. Gorgoi, F. Björefors, K. Edström and T. r. Gustafsson, *Chem. Mater.*, 2015, **27**, 2591–2599.
50 C. Liu, Z. G. Neale and G. Cao, *Mater. Today*, 2016, **19**, 109–123.
51 J.-H. Song, J.-T. Yeon, J.-Y. Jang, J.-G. Han, S.-M. Lee and N.-S. Choi, *J. Electrochem. Soc.*, 2013, **160**, A873–A881.
52 J. Heine, P. Hilbig, X. Qi, P. Niehoff, M. Winter and P. Bieker, *J. Electrochem. Soc.*, 2015, **162**, A1094–A1101.
53 T. Dong, J. Zhang, G. Xu, J. Chai, H. Du, L. Wang, H. Wen, X. Zang, A. Du and Q. Jia, *Energy Environ. Sci.*, 2018, **11**, 1197–1203.
54 Q. Zhang, J. Pan, P. Lu, Z. Liu, M. W. Verbrugge, B. W. Sheldon, Y.-T. Cheng, Y. Qi and X. Xiao, *Nano Lett.*, 2016, **16**, 2011–2016.
55 K. Xu, M. S. Ding, S. Zhang, J. L. Allen and T. R. Jow, *J. Electrochem. Soc.*, 2002, **149**, A622–A626.
56 J. Yi Wu, H. Xia Zeng, Q. Xuan Shi, X. Wei Li, Q. Xia, Z. Xue, Y. s. Ye and X. Lin Xie, *J. Power Sources*, 2018, **405**, 7–17.
57 X. Li, Z. Zhang, S. Li, L. Yang and S.-i. Hirano, *J. Power Sources*, 2016, **307**, 678–683.
58 Y. K. Sun, Z. Chen, H. J. Noh, D. J. Lee, H. G. Jung, Y. Ren, S. Wang, C. S. Yoon, S. T. Myung and K. Amine, *Nat. Mater.*, 2012, **11**, 942–947.
59 X. Fan, L. Chen, O. Borodin, X. Ji, J. Chen, S. Hou, T. Deng, J. Zheng, C. Yang and S.-C. Liou, *Nat. Nanotechnol.*, 2018, **13**, 715–722.
60 K. Chen, Y. Shen, J. Jiang, Y. Zhang, Y. Lin and C.-W. Nan, *J. Mater. Chem. A*, 2014, **2**, 13332–13337.